Available online at www.eccomasproceedia.org
Eccomas Proceedia COMPDYN (2021) 2965-2982

ECCOMAS
Proceedia

COMPDYN 2021
8th ECCOMAS Thematic Conference on
Computational Methods in Structural Dynamics and Earthquake Engineering
M. Papadrakakis, M. Fragiadakis (eds.)
Streamed from Athens, Greece, 28 - 30 June 2021

THE INFLUENCE OF WOODEN ROOF CONNECTION ON THE DYNAMIC AND EARTHQUAKE RESPONSE OF OLD INDUSTRIAL STONE MASONRY BUILDINGS

G.C. Manos[1] **and L. Kotoulas**[2]

[1] Professor Emeritus, Lab. Strength of Materials and Structures,Aristotle University
gcmanos@civil.auth.gr

[2] Post-graduate student, Lab. Strength of Materials and Structures, Aristotle University
lpkotoulas@gmail.com

Abstract

Unreinforced masonry made of stone and low strength mortar has been used for centuries in forming the structural system of old type buildings. Wooden roofs were also used as part of such structural systems. The influence of the connections of such wooden roofs with the vertical masonry walls is the objective of this study. A number of old stone-masonry buildings used as leather factories in the island of Samos-Greece are employed in this investigation. The wooden roofs of these buildings collapsed either partly or totally during the recent earthquake of October 2020. Initially, the dynamic behaviour typical forms of such buildings with wooden roofs are studied. A variation of the connections of such a wooden roof with the vertical stone masonry walls is studied in a parametric way. Next, the earthquake response of the same structural formations are also studied using again the variation of these connections as the main parameter. Towards this end earthquake design spectra are used as well as the acceleration recordings of this earthquake ground motion by an instrument located in the Samos island. Numerical simulation results are presented and discussed. Through the comparison of the obtained numerical predictions with the observed behaviour the validity of the numerical approach is discussed.

Keywords: Wooden roof, Stone masonry; weak mortar; Gravitational forces, Seismic actions,

ISSN:2623-3347
Peer-review under responsibility of the organizing committee of COMPDYN 2021.
doi: 10.7712/120121.8689.19524

1 INTRODUCTION

An earthquake occurred 16km North from the Greek island of Samos on the 30th of October 2020 (11:51GMT) with a magnitude of M6.7 (Fig. 1). This island is located at the East side of the Aegean Sea an area seismically active ([1], to [7]) The main event caused widespread structural damage mainly at numerous low-rise old unreinforced masonry buildings of this island. It all also caused heavy damage and collapse of multi-story reinforced concrete (R/C) buildings at the city of Izmir located at the coastline of mainland Turkey towards the North-East, approximately 60km from the epicenter of this earthquake. This study focuses on the effects of this seismic strong motion on the Greek island of Samos. The Institute of Engineering Seismology and Earthquake Engineering (ITSAK) operates a strong motion accelerograph at the city of Vathi, the capital of Samos. The ground accelerations at Vathi due to the main shock were recorded by this instrument (see preliminary report of ITSAK, [6] and ETAM [7]) having peak horizontal ground acceleration 227cm/sec2 and peak vertical ground acceleration 134cm/sec2.The main event was followed by a considerable number of aftershocks, with the aftershock sequence being still active. (Fig. 2).

Figure 1. Map indicating the epicenter of the 30th of October 2020 seismic event

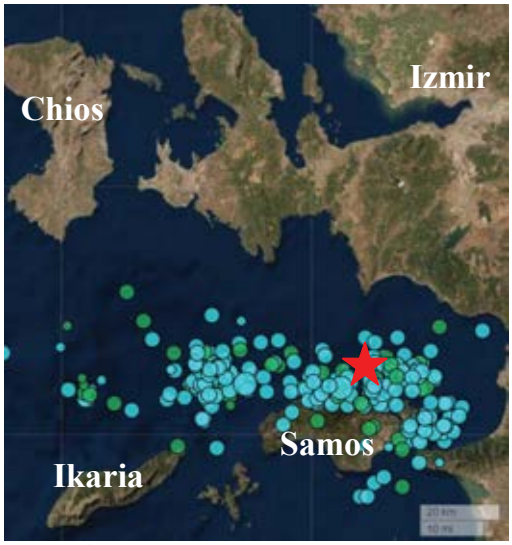

Figure 2. The epicenter of the 30th of October 2020 main event and the following aftershock sequence

The most spectacular structural damage could be observed at the two main cities in the island, its capital (Vathi) and Karlovaisi 25km to the West (Fig. 3). Due to the location of the epicen-

ter, having the same epicentral distance from both Vathi and Karlovasi, and due to the generating mechanism of this earthquake that followed an almost East-West fault line, as can be seen from the aftershock sequence, it can be reasonably assumed that the strong motion characteristics at Karlovasi would be quite similar to those of the recorded strong motion at Vathi. This assumption will be made use of in the section presenting selected numerical analyses predictions of the structural response of damaged buildings [8].

Figure 3. Map of the North cost-line of the island of Samos where the two main cities of Vathi and Karlovasi are located.

1.1 The recorded ground motion

In figure 3 the recordings of the earthquake ground motion, in terms of ground acceleration, velocity and displacement in the two horizontal directions are shown [6]. Due to the location of the epicenter, the same epicentral distance of both the city of Vathi and the city of Karlovasi from the epicenter (see figures 1, 2, 3) and due to the generating mechanism of this earthquake that followed the almost East-West fault line, as can be seen from the aftershock sequence it can be reasonably assumed that the strong motion characteristics at Karlovasi would be quite similar to those of the recorded strong motion at Vathi.

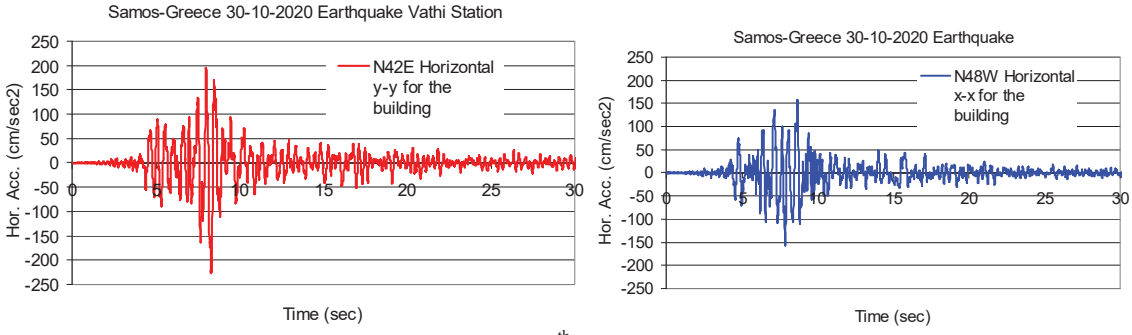

Figure 4. Horizontal ground acceleration recorded at 30th October 2020 at Vathi by an instrument managed by the Institute of Earthquake Engineering and Engineering Seismology (ITSAK, see reports [6] and [7]).

Figure 5 depicts the inelastic acceleration response spectral curves of the two horizontal components of the recorded ground motion at Vathi (Fig. 4) for 5% damping ratio and ductility factor m=1.5. In the same figure the design spectral curves as predicted by Euro-Code 8 are also shown. These design spectral curves were obtained for ground design acceleration equal to 0.24g (g= the acceleration of gravity) and for two different soil categories either soil C (flexible soil) or soil D (very flexible soil). This peak design ground acceleration is in accor-

dance with the seismic zoning map of Grrece [ ]. It is also assumed that the soil conditions near the coastline either at Vathi or at Karlovasi will belong to either one of these two soil conditions. Moreover, these design spectral curves are employing damping ratio equal to 5% and response modification factor q=1.5 (the same as the ductility factor value for the inelastic spectral cuves) and importance factor equal to 1 (γ=1). Finally, the design spectral curves are obtained for either type 1 or type 2 earthquake design motion, as specified by Euro-Code 8 [ ]. Type 2 is suppose to represent an earthquake hazard from an event with a magnitude lesser than M=5.5 on the Richter scale.

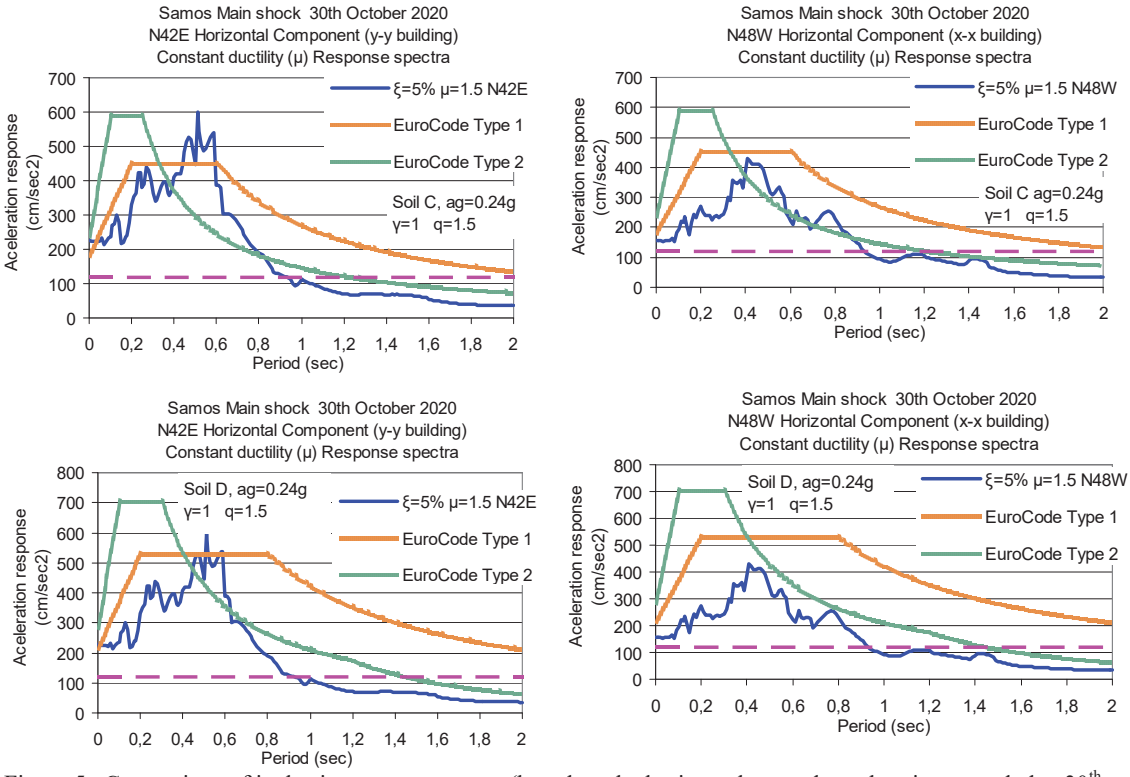

Figure 5. Comparison of inelastic response spectra (based on the horizontal ground acceleration recorded at 30th October 2020 at Vathi. [ ]) and Euro-code 8 design spectra.

From the comparison between these inelastic response spectra (based on the horizontal ground acceleration recorded at 30th October 2020 at Vathi and the corresponding Euro-code 8 design spectra (either Type 1 or 2 and either soil category C or D, [9] to [14]) the following observations can be made. **a)** Type 1 design spectra agree better with the inelastic response spectra (based on the recorded ground motion) than type 2 design spectra. **b)** The type 1 design spectra for soil category D have spectral acceleration amplitudes that are larger in almost all the plotted period range than the corresponding inelastic response spectra values (based on the recorded ground motion). **c)** The type 1 design spectra for soil category C have spectral acceleration amplitudes that are larger in almost all the plotted period range, apart from the period range between 0.45sec. and 0.61sec., than the corresponding inelastic response spectra values (based on the recorded ground motion).

2 ANALYSED STRUCTURES

In many Greek islands as well as at the old part of city-centers in many Greek cities a considerable number of old buildings still survives despite the destruction due to the military operations or the frequent earthquake activity. A considerable number of such buildings were demolished to give room to the extended urban development that took place after World War II and the tourism activity that followed, particularly in the islands. However, during the last four decades a conservation effort became quite strong endorsing a number of such building in a conservation register being under special legislative protection. In this category belong the buildings depicted in figures 6 and 7. These buildings were used as leather processing factories an activity that was prominent in Samos island from the end of the 9th century till World War II when started declining. A number of these buildings were left unoccupied and without any maintenance, which makes them vulnerable to strong earthquake excitations apart from the used construction system which unreinforced stone masonry walls covered by a wooden roof

Figure 6. Old industrial buildings under conservation status

Figure 7. Old industrial buildings (Tambakia) at the coastline of Karlovasi

The earthquake performance of this type of structures is dominated by certain response mechanisms that can be characterized as “global”. These mechanisms include a) the connection of the wooden roof to the masonry walls b) the interconnection of the masonry walls at the corners and c) the foundation deformability including the potential of partial uplifting at the foundation due to tensile forces arising from excessive overturning moment response and uneven foundation settlements (see [13], [17]). All these mechanisms are nonlinear in nature and it is many times difficult to quantify them in order to include their influ-

ence in realistic numerical approximations. An additional obstacle in the effort to evaluate in a realistic way the earthquake performance of these structures arises from the difficulty in assessing the actual strength of the materials and the structural elements built with these materials.

Figure 8. Map indicating the location of the damaged old industrial buildings in Karlovasi- Samos

In figure 4 the recordings of the earthquake ground motion, in terms of ground acceleration, velocity and displacement in the two horizontal directions are shown. Due to the location of the epicenter, the same epicentral distance of both the city of Vathi and the city of Karlovasi from the epicenter (see figures 1, 2, 3 and 8) and due to the generating mechanism of this earthquake that followed the almost East-West fault line, as can be seen from the aftershock sequence (figure 2) it can be reasonably assumed that the strong motion characteristics at Karlovasi would be quite similar to those of the recorded strong motion at Vathi. In the subsequent numerical simulation the inelastic acceleration response spectra values, obtained from the recorded ground acceleration at Vathi for response modification factor q=1.5, are employed. Based on the previous stated rational this earthquake excitation is believed to be a realistic approximation for the analysed structures located at the she-shore of Karlovasi, as indicated in figure 8. In the following a simplified numerical methodology is followed in order to predict the earthquake performance of the studied stone masonry industrial building. During past research a number of simple or complex numerical approaches have been applied for such vulnerable stone masonry structures damaged by past earthquakes ([15] to [30]).

2.1 Elastic numerical simulation

The numerical model of this industrial building with its wooden roof is depicted in figure 9. The wooden roof elements are connected with the masonry peripheral walls without transferring any bending moments. The stiffness of this connection is a parameter that is varied in this investigation. Summary results form various numerical dynamic spectral analyses are presented and discussed here. The numerical model of figure 9 represents a simplification of the Karlovasi leather processing factory depicted in figure 10, which can be seen being formed by two identical parts with respect to a longitudinal axis of symmetry parallel to x-x axis. At first, one of these parts is numerical simulated, as is shown in figure 9. Without verification of the actual geometry and the exact orientation of this building the length is assumed equal to 22.5m and 10m in the x-x and y-y directions, respectively. The height from ground level to

the top of the roof is assumed equal to 10m. Eight (8) trusses are assumed to form the wooden roof equally spaced along the x-x direction, as shown in figure 9. This wooden roof is connected to both the longitudinal walls at certain location though the transverse beams forming the bottom part of these wooden trusses. Moreover, This wooden roof is also connected by a series of longitudinal wooden beams with the gables of the two transverse wall (parallel to the y-y direction). In the subsequent numerical analysis the x-x direction is presumed to coincide with the N48W component of the recorded ground motion whereas the y-y direction with the N42E component.

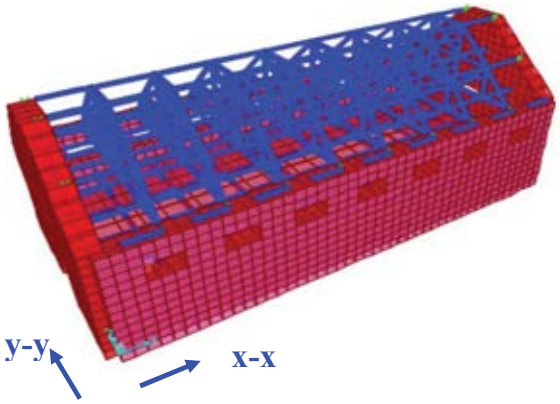

Figure 9. Simplified numerical model of a typical industrial building

10. A two-story twin industrial building of unreinforced masonry

As already mentioned, the influence of the connections of the wooden roof with the peripheral masonry walls is the objective of this parametric simplified numerical simulation. This is done as follows. Initially, the wooden beams are considered as pinned to the masonry walls, capable of transferring axial and shear forces (not bending moments) in a way that the displacements of the wooden end is the same as the point of the masonry wall it is connected to (rigid connection). Next, this connection is done through flexible 3-D links with limited stiffness thus allowing a relative displacement between the end of the wooden beam at its connecting location of the masonry wall. By decreasing the stiffness of these 3-D links the level of force that can be transferred between these two media can be limited. Moreover, by decreasing the stiffness of these 3-D links the restrain that is enforced by the interaction between the wooden roof and the masonry walls is also decreased. These effects will be shown in the following discussion. It should be recognized that is a simplification of the actual interaction that is a more complex non-linear mechanism than what is described here. Despite this simplification, the influence of such a flexible connection is being presented and discussed here.

2.2 Modal analysis.

Initially, the most significant eigen-modes of the simplified numerical model depicted in figure 9 having three different wooden-beam to masonry-wall connections is studied. As mentioned, these connections are: 1-Rigid, 2-Moderately flexible and 3-Flexible. The obtained modal shapes, modal periods and modal mass participation ratio values are presented in what follows.

1-Rigid connections

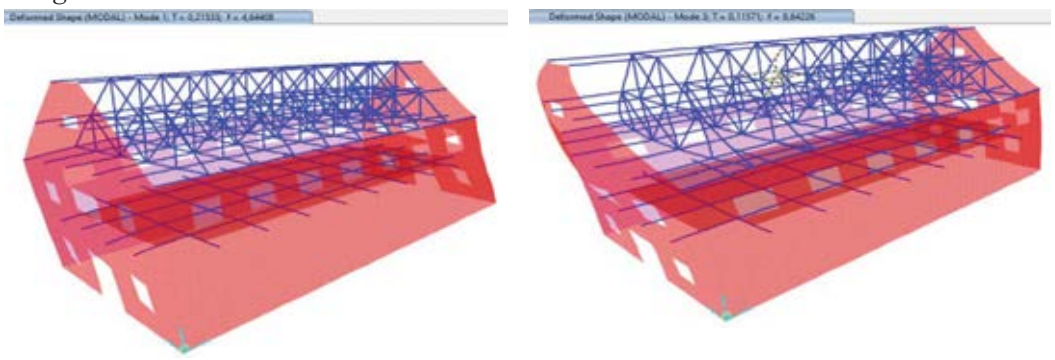

T1=0.215sec Ux=0.0% Uy=83.0% **T3=0.116sec Ux=57.1% Uy=0.0%**

2-Moderately flexible connections

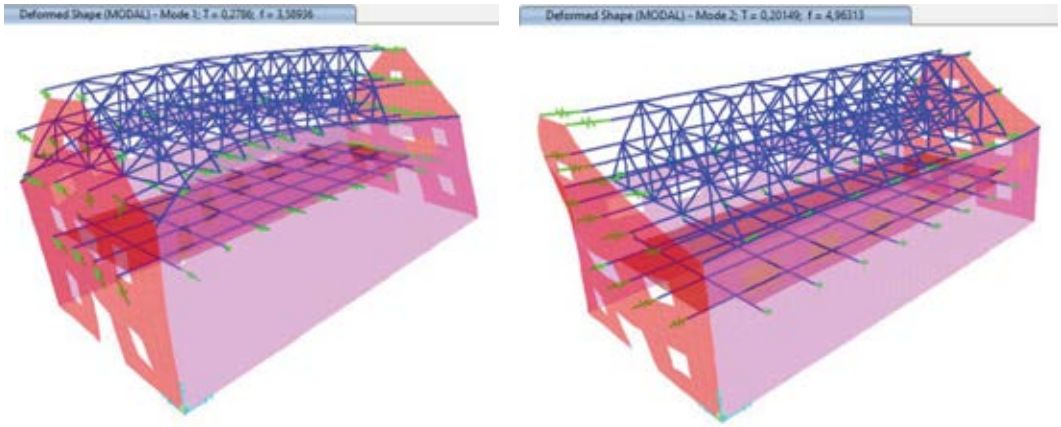

T1=0.279sec Ux=0.0% Uy=61.4% **T3=0.201sec Ux=32.6% Uy=0.0%**

3-Flexible connections

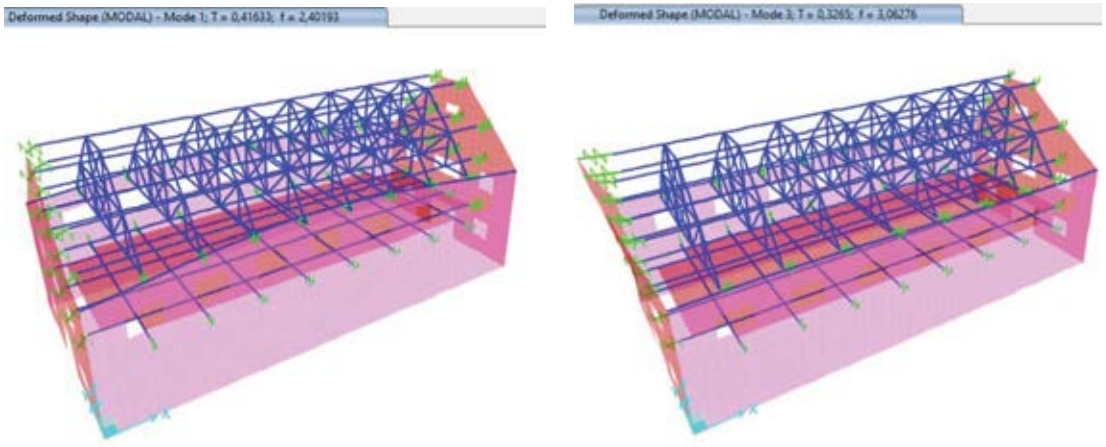

T1=0.416sec Ux=0.0% Uy=48.5% **T3=0.327sec Ux=23.7% Uy=0.0%**

Figure 11. Eigen-modes for the simplified numerical model of the industrial building for Rigid, Moderately flexible and Flexible connections between the wooden roof beams and the masonry walls.

The following summarize the influence of the attempted simplified relaxation of the connections between the wooden roof beams and the masonry walls on the dynamic characteristics of the studied structural system.

a) As expected, the increase in the flexibility of the connections between the wooden roof beams and the masonry walls results in an increase of the corresponding eigen-period values of the studied system from 0.215 sec. to 0.416 sec. for the mainly translational eigen-mode in the transverse y-y direction and from 0.116sec. to 0.327 sec. for the mainly translational eigen-mode in the longitudinal x-x direction.
b) The increase in the flexibility of the connections between the wooden roof beams and the masonry walls results in a decrease in the corresponding modal mass participation ratio value. This is pronounced for the transverse y-y translational 1st eigen-mode (from 83% to 48.5%) but even more pronounced for the longitudinal x-x translational 3rd eigen-mode (from 57.1% to 23.7%).

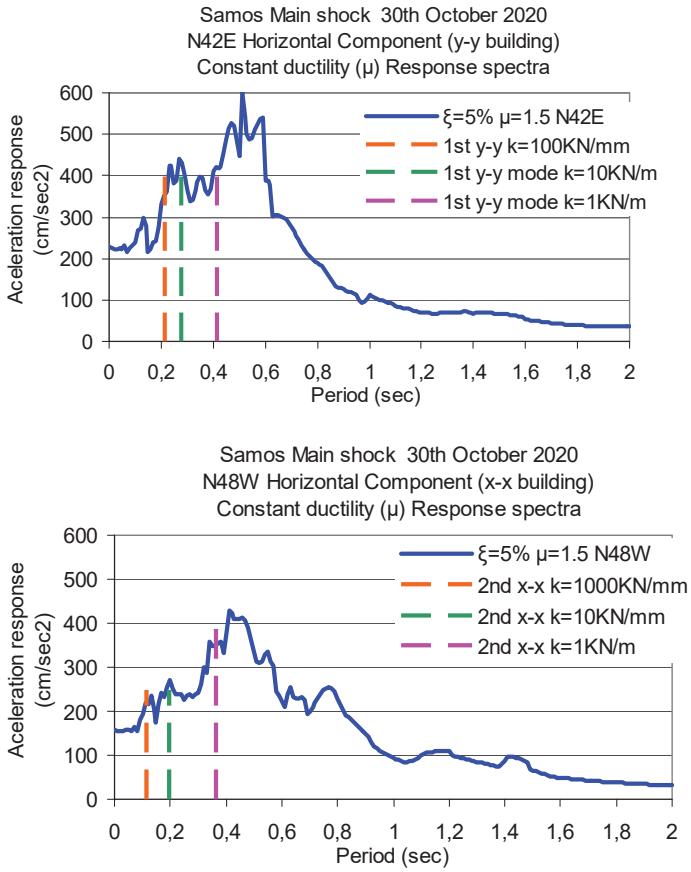

Figure 12. Inelastic acceleration response spectral curves (m=1.5) based on the recorded ground acceleration together with the variation of the eigen-periods for the main y-y and x-x translational eigen-modes as they resulted from the simplified numerical model of the industrial building for Rigid, Moderately flexible and Flexible connections between the wooden roof beams and the masonry walls.

In figure 12 the variation of the eigen-periods for the main y-y and x-x translational eigen-modes, as they resulted from the simplified numerical model of the industrial building for Rigid, Moderately flexible and Flexible connections between the wooden roof beams and

the masonry walls, are plotted together with the corresponding inelastic acceleration response spectral curves (m=1.5). These inelastic acceleration spectral curves are based on the recorded ground acceleration together for the Samos island earthquake (30th October 2020). As can be seen from these plots the increased flexibility of the connections between the wooden beam roofs and the masonry walls will also result in an increase of the corresponding spectral acceleration value thus leading to a relevant increase on the seismic force levels for the studied structure. At the same time these increased inelastic spectral acceleration values are more in agreement with the corresponding Euro-Code 8 design spectral values, as already discussed on the basis of figure 5, than those of the rigid connections.

3 NUMERICAL EARTHQUAKE PERFORMANCE

In this section the numerical earthquake performance of the studied structure is presented in terms of a) maximum displacement values at the top of the masonry walls b) maximum normal and shear stress values of the masonry walls c) maximum axial force values that developed at the connections between the wooden roof beams and the masonry walls. All these values were obtained through dynamic spectral elastic analysis using the inelastic spectral curves depicted in figure 12. The presented results are for two specific load combinations:

1st Load Combination: Dead + ResSp N42E + 0.3 ResSp N48W
2nd Load Combination: Dead + ResSp N42E + 0.3 ResSp N48W

Dead= The dead load of the masonry walls and the roof.

ResSp N42E = The earthquake forces resulting from the dynamic spectral analysis in the y-y (transverse direction).

ResSp N48W = The earthquake forces resulting from the dynamic spectral analysis in the x-x (longitudinal direction)

As was done for the modal analysis the earthquake performance is examined utilizing the simplified numerical model depicted in figure 9 having the described before three different wooden-beam to masonry-wall connections (e..g. 1-Rigid, 2-Moderately flexible and 3-Flexible). In figure 13 includes the results obtained from the simplified numerical simulation assuming rigid connections of the wooden roof beams with the masonry walls. In figure 13a and 13b the displaced masonry walls of the structure are depicted in figures 13a and 13b for load combinations with the seismic forces applied either mainly in the transverse N42E or mainly in the longitudinal N48W directions, respectively. Figures 13c depicts the normal stress (S22) distribution whereas figure 13d the shear stress (S12) distribution for a load combination with the seismic forces applied mainly along the transverse N42E direction. Figure 13e depicts the normal stress (S22) distribution for a load combination with the seismic forces applied mainly along the longitudinal N48W direction. Figure 13f depicts the distribution of the axial forces that develop at the roof wooden beams for a load combination with the seismic forces applied mainly along the transverse N42E direction whereas figure 13g depicts the axial forces that develop at the roof wooden beams for a load combination with the seismic forces applied mainly along the longitudinal N48W direction. The results for moderately flexible (figures 14) or for flexible connections (figure 15) are also shown.

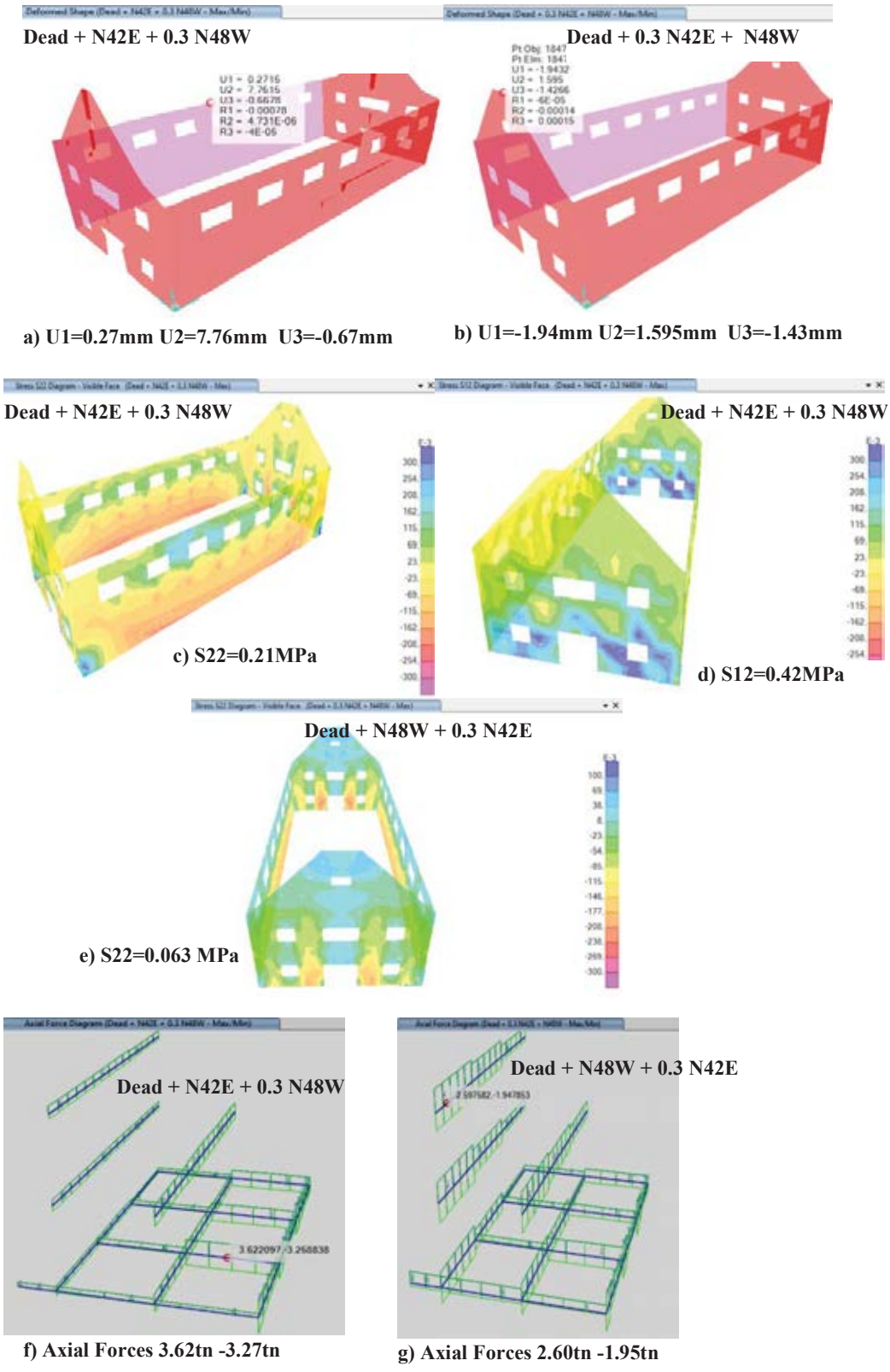

Figure 13. Structural response results. Rigid connections of the wooden roof beams with the masonry walls

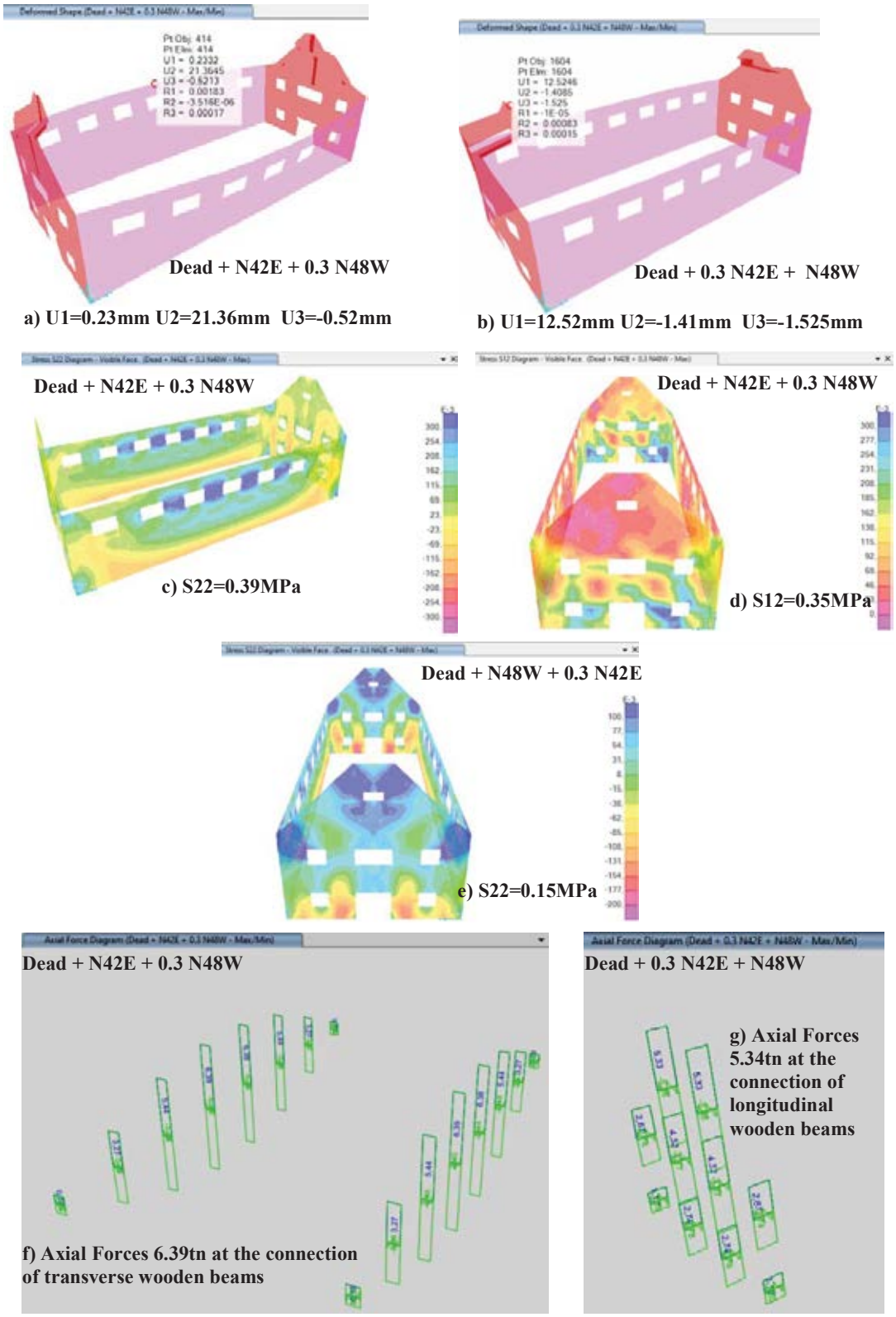

Figure 14. Structural response results. Moderately flexible connections of the wooden roof beams with the masonry walls

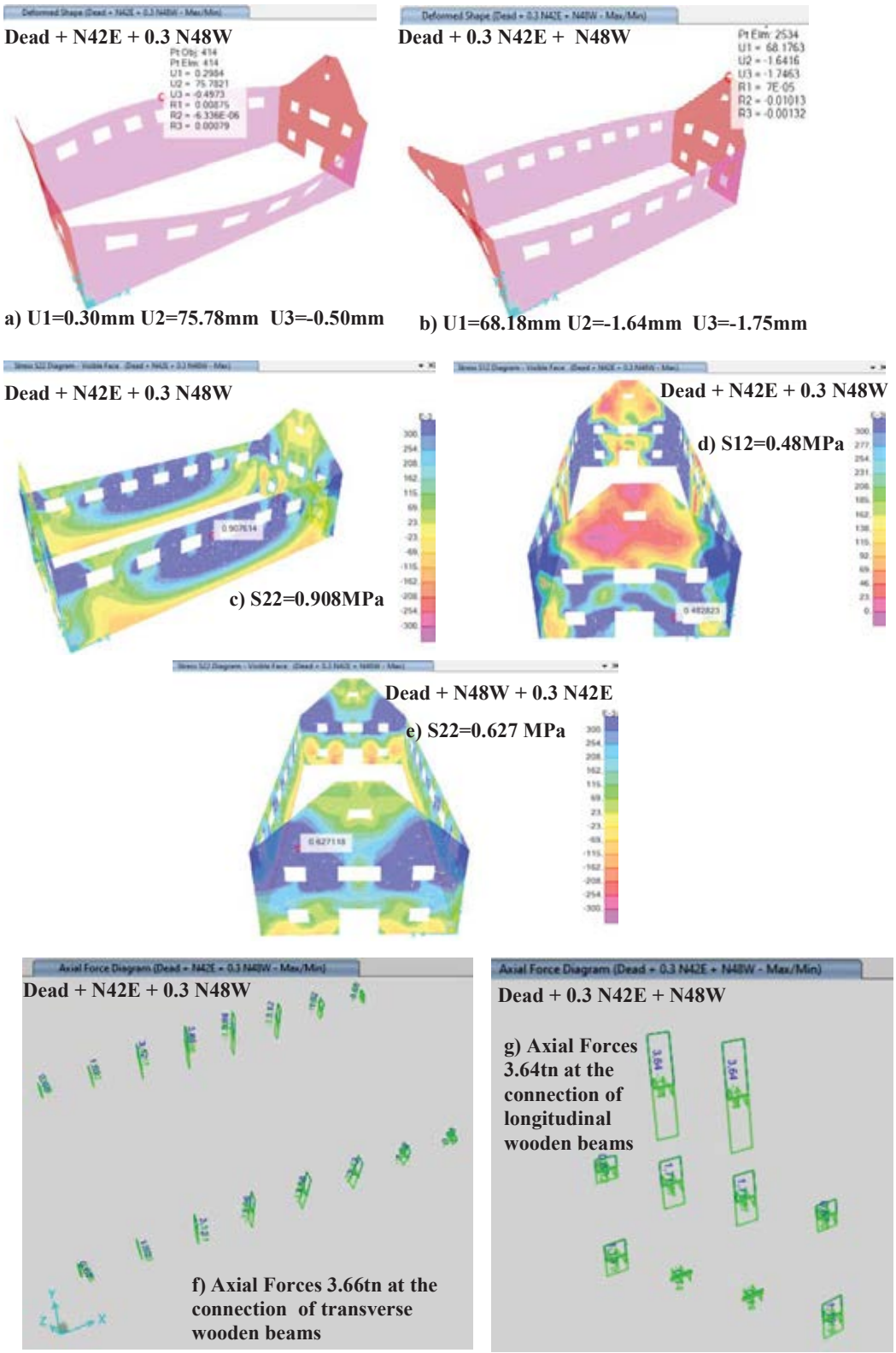

Figure 15. Structural response results. Flexible connections of the wooden roof beams with the masonry walls

Table 1. Peak values of the response parameters resulting from the simplified numerical analyses

Numerical Model-Roof Connection cases	Out of plane y-y displ. of longitudinal walls (mm)	Out of plane x-x displ. of Transverse walls (mm)	Normal stress Longit. Walls S22 (MPa)	Normal stress Transv. Walls S22 (MPa)	Shear stress Longit. Walls S12 (MPa)	Axial or connection forces Transv. Beams (tn)	Axial or connection forces Longit. Beams (tn)
(1)	(2)	(3)	(4)	(6)	(5)	(7)	(8)
Rigid Qy=352tn Qx=175tn	7.76	1.94	0.21	0.063	0.42	3.62	2.60
Moderately Flexible Qy=306tn Qx=195tn	21.36	12.52	0.39	0.15	0.35	6.39 / 6.39mm*	5.34 / 5.34mm*
Flexible Qy=372tn Qx=259tn	75.78	68.18	0.908	0.627	0.48	3.66 / 36.6mm*	3.64 / 36.4mm*

* the relative axial displacement between the wooden roof beam and the masonry wall at the location of their connection

Table 1 summarizes all the peak response values from the results plotted in figures 13, 14 and 15. In the first column of this table each of the three analyzed cases of connection between the wooden roof beams and the masonry walls is denoted. At the same column the peak horizontal base shear values are also listed for each case, as they resulted from the dynamic spectral (see figure 12) analyses along the x-x (N48W perpendicular to the transverse walls) and y-y (N42E perpendicular to the longitudinal walls) directions (see figure 9). As already discussed, because of the variation of the amplitudes of the employed inelastic spectral curves with the eigen periods values (figure 12) the structural system with the flexible roof-to-masonry connections is subjected to the highest seismic force amplitudes in both x-x and y-y directions. Consequently, part of the significant amplification of the obtained displacement and stress response for this case as compared with the cases of either the rigid or the moderately flexible connections is partly due to this fact. However, another large part of this amplification must be attributed to the fact that the flexible connections exercise limited restrain in prohibiting the masonry walls to displace, especially in the out-of-plane direction. This is evident by comparing the out-of-plane peak displacement values of either at the top of the longitudinal walls (column 2 of table 1) or at the top of the transverse walls (column 3 of table 1). As can be seen, an increase flexibility in these wooden roof beam to masonry wall connections result in a large increase in the out-of-plane displacements at the top of either the longitudinal or the transverse masonry walls. This in turn results in a corresponding increase in the peak (tensile) axial stress values normal to the bed joints (S22) for either the longitudinal masonry walls (column 4 of table 1) or the transverse masonry walls (column 5 of table 1). In contrast, the moderate variation in the peak shear stress value of the transverse masonry walls is in line with the corresponding variation of the base shear value in the y-y direction (Qy, column 1 of table 1). Finally, the increase in the flexibility of the wooden roof beam to masonry wall connections result in a decrease, as expected, in the axial force value that is transmitted through these connections (columns 7 and 8 table 1). It is also interesting to note that the rigid connections between the wooden roof beams and the masonry walls, which is an unrea-

listic ideal case, results in relatively small out-of-plane displacement values, despite the fact that the resulting axial forces at the connection locations are also relatively small. On the contrary, the increase in the flexibility of these connections from moderately flexible to flexible results in a decrease at the level of axial force which is in agreement with the resulting increase of the out-of-plane displacement at the top of the masonry walls. In columns 7 an 8 of table 1 the relative axial displacement between the wooden roof beam and the masonry wall at the location of their connection is also listed. As can be seen, the increase flexibility of this connection means in a sense a large relative displacement between the wooden roof beam and the masonry wall. This practically means that there is a possibility of a loss of support of the wooden roof beam when this relative displacement becomes excessive, as is the case of the flexible connection assumed in this simplified numerical simulation. This is the case portrayed by the collapsed roof in figures 7 and 10. Obviously, this simplified analysis is only qualitative. In order to obtain realistic numerical predictions it is necessary to include in the numerical analysis a valid numerical description of the non-linear connection mechanism ([31] to [36]).

4 CONCLUSIONS

- The recent earthquake sequence in the Greek island of Samos gave the opportunity of assessing the earthquake performance of various types of structure in Greece. It can be stated that the enforcement in 1995 of the "New Greek Seismic Code" together with the provisions of the Euro-Codes has substantially increased the safety level of structures against earthquakes. A significant expansion of the strong motion network of accelerographs that covers the whole of Greece provides very important information on the characteristics of the earthquake strong ground motion that is very useful in assessing the consequences of the intense earthquake activity to the built environment. The relevant data base is enriched with valuable information on the characteristics of the earthquake strong ground motion that is very useful to designers and contractors.
- A source of seismic risk that can result in human loss was highlighted by this earthquake event. It is generated by old and weak unreinforced masonry structures which are left unoccupied and not maintained by their owners due to various social-economic non-incentives and complications. This category includes numerous old building that belong to culture heritage being listed in conservation status. The group of old stone- masonry buildings with wooden roof that were used a leather processing factories at Karlovasi-Samos belong to this category.
- Numerical tools combined with realistic measurements of the seismic forces generated by a strong earthquake ground motions can be utilized to explain the observed structural damage. They can also be utilized in the subsequent retrofitting effort. Towards this objective, the present numerical study investigated the influence of the flexibility of the connections between the wooden roof beams and the masonry walls of such old stone masonry industrial buildings.
- The flexible connections exercise limited restrain in prohibiting the masonry walls to displace, especially in the out-of-plane direction. Consequently, such increased flexibility results in relatively large displacement and stress response demand for the masonry walls that could be detrimental leading to mainly flexural type failures. This is to be expected for masonry construction with low flexural capacities. At the same time, the increase in the flexibility of these connections results in a decrease of the level of axial force which

is in agreement with the resulting increase of the out-of-plane displacement at the top of the masonry walls.

- At the same time, the increased flexibility of wooden roof beams to masonry wall connections also results in large relative displacement between the wooden roof beam and the masonry walls. This practically means that there is a possibility of a loss of support of the wooden roof beam when this relative displacement becomes excessive, as is the case of the flexible connection assumed in this simplified numerical simulation.
- The present simplified analysis is only qualitative. In order to obtain realistic numerical predictions it is necessary to include in the numerical analysis a valid numerical description of the non-linear connection mechanisms. Moreover, there is also need to obtain measured capacities of such connections through laboratory measurement focusing to this problem.

REFERENCES

[1] Ambrazeys, N.N. et.al. “Prediction of Horizontal Response Spectra in Europe” Int. J. of Earth. Engin. and Struct. Dyn., pp. 371-400, Vol. 25, No. 4, April 1996.

[2] Ambrazeys, N.N. et.al. “Prediction of Vertical Response Spectra in Europe” Int. J. of Earthquake Engineering and Structural Dynamics, pp. 401-414, Vol. 25, No. 4, April 1996.

[3] Carydis, P.G., Tilford, N.R., Brandow, G.E. and Jirsa, J.O. "The Central Greece Earthqaukes of February-March 1981, A Reconnassance and Engineering Report", National Academy Press, Washington, D.C., Report No. CETS-CND-018, pp 162, 1982.

[4] Papazachos, B.C. (1990) "Seismicity of the Aegean and the Surrounding Area", Tectonophisics, 178, 287-308.

[5] Manos G.C., “Consequences on the urban environment in Greece related to the recent intense earthquake activity”, Int. Journal of Civil Engineering and Architecture, Dec. 2011, Volume 5, No. 12 (Serial No. 49), pp. 1065–1090.

[6] The Earthquake of Oct. 30, 2020, M6.7 (11:51GMT) North of Samos Island (Greece): Observed strong ground motion on Samos island. Institute of Earthquake Engineering and Engineering Seismilogy (ITSAK) , Preliminary report, October 2020.

[7] Prelimiray report on the Samos 30th October 2020 earthquake. Hellenic Society of Earthquake Engineering, ETAM,-report- Samos-2020 earthquake, November 2020.

[8] Manos G.C. “The 30th of October Samos-Greece Earthquake. Issues Relevant to the Protection from Structural Damage Caused by Strong Earthquake Ground Motions”, Journal of Architecture and Engineering, Volume 5 Issue 4 (2020), eISSN: 2500-0055, http://aej.spbgasu.ru/

[9] Paz. M. International Handbook of Earthquake Engineering: "Codes, Programs and Examples", edited by Mario Paz, Chapter 17, Greece by G.C. Manos, Chapman and Hall, ISBN 0-412-98211-0, 1994.

[10] Organization of Earthquake Planning and Protection of Greece (OASP),. (2001).Guidelines for Level- A earthquake performance checking of buildings of public occupancy», Athens.

[11] Organization of Earthquake Planning and Protection of Greece (OASP), (2011). Guidelines for Retrofitting in Reinforced Concrete Buildings, Athens.

[12] EAK-2000 Greek seismic Code.

[13] Provisions of Greek Seismic Code with revisions of seismic zonation", Government Gazette, Δ17α /115/9/ΦΝ275, No. 1154, Athens, 12 Aug. 2003.

[14] ELOT EN 1998-1/2005-05-12, Eurocode 8: Design of structures for earthquake resistance - Part1: General rules, seismic actions and rules for buildings.

[15] Croci G., "The Conservation and Structural Restoration of Architectural Heritage", Computational Mechanics Publication, 1998, ISBN 1 85312 4826.

[16] Limoge Schraen C., Giry C., Desprez C., Ragueneau F., "Tools for a large-scale seismic assessment method of masonry cultural heritage", Structural Studies, Repair and Maintenance of Cultural Heritage, STREMAH XIV, WIT press (2015), ISBN 978-1-84564-968-5.

[17] Lagomarsino Sergio "Damage assessment of churches after L'Aquila earthquake (2009)" Bulletin of Earthquake Eng. 2011, DOI 10.1007/s10518-011-9307-x.

[18] Modena C. et.al., " L'Aquila 6th April 2009 Earthquake: Emergency and Post-emergency Activities on Cultural Heritage Buildings" Claudio Modena C. et.al. , Chapter 20, Earthquake Engineering in Europe, Geotechnical, Geological, and Earthquake Engineering 17, DOI 10.1007/978-90-481-9544-2_20, Springer Science+Business Media B.V. 2010.

[19] Manos G.C. and Papanaoum E., "Earthquake Behaviour of a R/C Building Constructed in 1933 before and after its Repair" STREMAH 2009, Tallin, 22-24 June, 2009.

[20] Manos G.C., Soulis V., Diagouma A. (2008) "Numerical Investigation of the behavior of the church of Agia Triada, Drakotrypa, Greece", Journal in Advances in Engineering Software 39 (2008) 284-300.

[21] Manos G.C., Soulis V. J & Karamitsios N., "The Performance of Post-Byzantine churches during the Kozani-1995 Earthquake – Numerical Investigation of their Dynamic and Earthquake Behaviour", 15WCEE, 2012, Portugal.

[22] Manos G.C. & Karamitsios N., "Numerical simulation of the dynamic and earthquake behavior of Greek post-Byzantine churches with and without base isolation", Earthquake Engineering Retrofitting of Heritage Structures, Design and evaluation of strengthening techniques, pp. 171-186, Edited By: S. Syngellakis, Wessex Institute of Technology, UK, ISBN: 978-1-84564-754-4, eISBN: 978-1-84564-755-1, 2013.

[23] Manos G.C., Kotoulas L., Felekidou O., Vaccaro S. and Kozikopoulos E. "Earthquake damage to Christian Basilica Churches – Application of an expert system for the preliminary in-plane design of stone masonry piers" , STREMAH-2015, A Coruna, Spain, 13-15 July, 2015.

[24] Manos G.C., "The Seismic Behaviour of Stone Masonry Greek Orthodox Churches" Journal of Architecture and Engineering, Vol. 1, Issue 1, March 2016, pp. 44-53, https://aej.spbgasu.ru/index.php/AE/index

[25] Manos G.C., Kotoulas L., Matsou V., Felekidou O. "Dynamic and Earthquake Behaviour of Greek Post-Byzantine Churches with Foundation Defornability – Experimental Investigation of Stone Masonry Materials Properties", Springer Publishing, I. N. Psy-

charis (seds.), I.N. Psycharis et al. (eds.), Seismic Assessment, Behavior and Retrofit of Heritage Buildings and Monuments, Computational Methods in Applied Sciences 37, DOI 10.1007/978-3-319-16130-3_9.

[26] Manos G., Kozikopoulos E., Kotoulas L., Soulis V. "The Earthquake performance of stone masonry Basilica churches in Kefalonia-Greece including wall detachment and soil foundation deformability", 16th European Conf. Earthquake Engineering, Thessaloniki-Greece, 2018.

[27] Kotoulas L., Manos G.C. "Unreinforced stone masonry churches in Greece under gravitational and earthquake actions", 7th ECCOMAS Thematic Conference on Computational Methods in Structural Dynamics and Earthquake Engineering M. Papadrakakis, M. Fragiadakis (eds.), Crete, Greece, 24–26 June 2019.

[28] Manos G.C., Kotoulas L., and Kozikopoulos E., (2019) "Evaluation of the Performance of Unreinforced Stone Masonry Greek "Basilica" Churches When Subjected to Seismic Forces and Foundation Settlement", Buildings 2019, 9, 106; doi:10.3390/buildings9050106.

[29] Manos GC & L Kotoulas. Unreinforced Stone Masonry Churches under Gravitational and Earthquake Actions, CompDyn 2019, Crete, Greece 2019.

[30] Soulis V. J. and Manos G. C., Numerical Simulation and Failure Analysis of St. Konstantinos Church, after the Kozani Earthquake", International Journal of Civil Engineering (2019) 17:949–967, https://doi.org/10.1007/s40999-018-0345-5

[31] Manos, George C., Clough, Ray W., Mayes, Ronald L "Shaking table study of single-story masonry houses: dynamic performance under three component seismic input and recommendations", Report UCB/EERC-83/11.

[32] Gulkan P., Clough R.W., Manos G.C. and Mayes R.L. "Seismic Testing of Single-story Masonry Houses : Part 1", Journal of Str. Eng. ASCE, Vol. 116, No 1, January 1990, pp. 235-256.

[33] Gulkan P., Clough R.W., Manos G.C. and Mayes R.L. "Seismic Testing of Single-story Masonry Houses : Part 2", Journal of Str. Eng. ASCE, Vol. 116, No 1, January 1990, pp. 257-274.

[34] Manos G.C., Mpoufidis D., Zafiriou Th, "The seismic behaviour of a Pre-cast R/C industrial complex subjected to the 1999 Athens-Greece Earthquake", 16th European Conf. Earthquake Engineering, Thessaloniki-Greece, 2018.

[35] European Committee for Standardization, Eurocode 6; "Design of Masonry Structures, Part 1-1:General Rules for Building. Rules for Reinforced and Unreinforced Masonry", EN 1996-1-1:2005.

[36] Katakalos K.V., Arnaoutis I., and Manos G.C. "Identification of failure mechanism of the Ottoman bath (Hamam) at Apollonia (Pazarouda) – Exploitation of historical data", Joural Case Studies in Construction Materials, 2020.